International Journal of Multiphase Flow 179 (2024) 104922

Contents lists available at ScienceDirect

International Journal of Multiphase Flow

journal homepage: www.elsevier.com/locate/ijmulflow

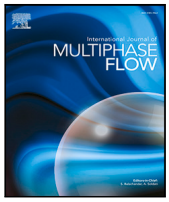

Three approaches to modelling heating and evaporation of monocomponent droplets

Dmitrii V. Antonov [a], Simona Tonini [b], Gianpietro Elvio Cossali [b], Mansour Al Qubeissi [c], Pavel A. Strizhak [a], Sergei S. Sazhin [a,b,d,*]

[a] Heat and Mass Transfer Laboratory, National Research Tomsk Polytechnic University, Tomsk 634050, Russian Federation
[b] Department of Engineering and Applied Sciences, Università degli Studi di Bergamo, Viale Marconi 6, 24044 Dalmine (BG), Italy
[c] College of Engineering Technology, University of Doha for Science and Technology, Doha 24449, Qatar
[d] School of Architecture, Technology and Engineering, Advanced Engineering Centre, University of Brighton, Brighton, BN2 4GJ, United Kingdom

ARTICLE INFO

Keywords:
Droplets
Heating
Evaporation
Mathematical model
Experimental measurements

ABSTRACT

Three approaches to modelling the heating and evaporation of monocomponent droplets are compared. Firstly, the heat rate supplied to the droplets to raise their internal energy is calculated based on the observation that steady-state equations for heat and mass balance in the gas phase should lead to the same droplet evaporation rates. The direct calculation of the above-mentioned heat rate is used in the second approach; the value of this rate is then used for the estimation of the droplet evaporation rate using the Spalding heat transfer number. In the third approach, the same algorithm as in the second approach is used to calculate the heat rate but the mass evaporation rate in this approach is inferred from the coupled solution to the momentum, mass and energy conservation equations in the gas phase; the gas mixture density in this approach depends on temperature. The predictions of the numerical algorithms for these approaches are compared with experimentally observed time dependencies of the rates of change of radii and average temperatures of n-decane droplets at initial temperatures and radii equal to 300 K and 0.85 mm, respectively, placed in a gas at temperatures 500 K and 760 K. It is shown that the algorithm for the third approach predicts values which are close to the experimental data.

1. Introduction

The importance of accurately modelling the heating and evaporation of droplets is well known and has been described in numerous papers and books starting with the pioneering monographs by Fuchs (1959) and Spalding (1963). These processes have a wide range of industrial applications, including spray combustion (Saha et al., 2012; Kitano et al., 2014) and drying (Barrow and Pope, 2007), pharmaceutical applications (Aliseda et al., 2008; Vehring et al., 2007), materials processing with micro-structures and crystal growth (Wolf et al., 2008; Kumar et al., 2010). The most recent achievements are discussed by Sazhin (2022). Amongst those papers published since Sazhin (2022), Xi et al. (2023), Fan et al. (2024), Zhang et al. (2024) are particularly noteworthy.

It is certainly not our intention to present an extensive review of the droplet heating and evaporation models developed so far (an attempt to do this was made by Sazhin (2022)). Instead, our focus will be on the models most widely used in engineering applications, and one of those most recently developed, which has been largely overlooked by the engineering community despite its clear advantages compared with previously developed models.

In one of the early but still widely used models, stationary droplet evaporation rate $\dot{m}_d \leq 0$ is expressed as a function of the Spalding mass transfer number $B_M = (Y_{vs} - Y_{v\infty})(1 - Y_{vs})^{-1}$ (Abramzon and Sirignano, 1989; Sazhin, 2022):

$$\dot{m}_d = -4\pi R_d D_v \rho_{\text{total}} \ln\left(1 + B_M\right), \tag{1}$$

where Y_{vs} and $Y_{v\infty}$ are vapour mass fractions close to droplet surfaces and away from them, R_d is the droplet radius, D_v is the vapour/gas diffusion coefficient, and $\rho_{\text{total}} = \rho_g + \rho_v$ is the density of the mixture of vapour and gas, assumed to be constant.

An alternative expression for $\dot{m}_d$ follows from the steady-state heat balance equation and is presented as (Abramzon and Sirignano, 1989;

* Corresponding author at: School of Architecture, Technology and Engineering, Advanced Engineering Centre, University of Brighton, Brighton, BN2 4GJ, United Kingdom.
E-mail address: S.Sazhin@brighton.ac.uk (S.S. Sazhin).

https://doi.org/10.1016/j.ijmultiphaseflow.2024.104922
Received 29 March 2024; Received in revised form 18 June 2024; Accepted 18 July 2024
Available online 23 July 2024

Nomenclature

Bi	Biot number [–]
$B_{M(T)}$	Spalding mass (heat) transfer number [–]
c	Specific heat capacity [J/(kg K)]
D	Diffusion coefficient [m^2/s]
Fo	Fourier number [–]
h	Convective heat transfer coefficient [W/(m^2 K)]
h_0	Parameter introduced in Expression (6) [–]
k	Thermal conductivity [W/(m K)]
L	Specific heat of evaporation [J/kg]
Le	Lewis number [–]
$\dot{m}_d$	Mass evaporation rate [kg/s]
$\hat{m}_e$	Normalised mass evaporation rate introduced in Expression (9) [–]
M	Molar mass [kg/kmole]
p	Pressure [Pa or bar]
$\dot{q}$	Heat rate transferred to the droplet [W]
q_n	Parameter introduced in Expression (6) [–]
R_d	Droplet radius [m]
R_u	Universal gas constant [J/(mole K)]
t	Time [s]
T	Temperature [K]
υ_n	Eigenfunctions introduced by Expression (6) [–]
Y	Mass fraction [–]

Greek symbols

ε	Parameter defined by Expression (10) [–]
κ_R	Parameter introduced in Expression (6) [1/s]
λ_n	Eigenvalues [–]
μ_0	Parameter introduced in Expression (6) [K]
ρ	Density [kg/m^3]
τ	Dimensionless time [–]
φ	Parameter defined by Expression (5) [–]

Subscripts

cr	Critical
d	Droplet
e	Evaporation
g	Ambient gas (air)
l	Liquid
p	Constant pressure
s	Surface
v	Vapour
0	Initial
∞	Ambient

Sazhin, 2022):

$$\dot{m}_d = -\frac{4\pi k_g R_d}{c_{pv}} \ln(1 + B_T), \tag{2}$$

where the Spalding heat transfer number is defined as

$$B_T = \left[c_{pv}(T_g - T_s)\right] \times \left\{ L - \frac{\dot{q}_d}{\dot{m}_d} \right\}^{-1}, \tag{3}$$

c_{pv}, k_g, and L are the vapour specific heat capacity, gas thermal conductivity, and specific heat of evaporation (estimated at the droplet surface temperature T_s), respectively; $\dot{q}_d > 0$ is the heat rate transferred inside the droplet (to raise its internal energy).

The expression for $\dot{q}_d$ follows from the requirement that $\dot{m}_d$ predicted by (1) and (2) should be the same:

$$\dot{q}_d = -\dot{m}_d \left[\frac{c_{pv}\Delta T}{B_T} - L \right] = -\dot{m}_d \left[\frac{c_{pv}\Delta T}{(1 + B_M)^{\varphi} - 1} - L \right], \tag{4}$$

where

$$\varphi = \left(c_{pv}/c_{pg}\right) \mathrm{Le}^{-1}, \tag{5}$$

$\Delta T = T_g - T_s$, $\mathrm{Le} = k_g/(c_{pg} D_v \rho_{\mathrm{total}})$ is the Lewis number, and c_{pg} and D_v are the ambient gas specific heat capacity and diffusion coefficient, respectively.

It was noticed (see Sazhin et al. (2014)) that $\dot{q}_d$ predicted by Expression (4) is different from that inferred from direct differentiation of the analytical expression for temperature distribution inside a spherically symmetric droplet:

$$\dot{q}_d = 4\pi R_d k_l \sum_{n=1}^{\infty} \left\{ q_n \exp\left[-\kappa_R \lambda_n^2 t\right] - \frac{\sin\lambda_n}{\| \upsilon_n \|^2 \lambda_n^2} \mu_0(0) \exp\left[-\kappa_R \lambda_n^2 t\right] - \right.$$

$$\left. - \mathcal{M} \sin\lambda_n \| \upsilon_n \|^{-2} \lambda_n^{-2} \right\} \left[-1 - h_0\right] \sin\lambda_n, \tag{6}$$

where

$$\mathcal{M} = \int_0^t \frac{\mathrm{d}\mu_0(\tau)}{\mathrm{d}\tau} \exp\left[-\kappa_R \lambda_n^2 (t - \tau)\right] \mathrm{d}\tau,$$

λ_n are solutions to the equation:

$$h_0 \sin\lambda + \lambda \cos\lambda = 0, \tag{7}$$

$$\| \upsilon_n \|^2 = \frac{1}{2} - \frac{\sin 2\lambda_n}{4\lambda_n} = \frac{1}{2} + \frac{h_0}{2(h_0^2 + \lambda_n^2)},$$

$$q_n = R_d^{-1} \| \upsilon_n \|^{-2} \int_0^{R_d} \tilde{T}_0(R) \sin\left[\lambda_n \left(R/R_d\right)\right] \mathrm{d}R,$$

$$\kappa_R = \frac{k_l}{c_l \rho_l R_d^2}, \ \mu_0(t) = h T_g(t) R_d k_l^{-1},$$

$\tilde{T}_0(R) = R T_{d0}(R)/R_d$, $h_0 = (h R_d/k_l) - 1$. The solution to (7) gives a set of positive eigenvalues λ_n ($n = 1, 2, \ldots$), ρ_l is the liquid density,

$$h = 2 k_g R_d^{-1} B_T^{-1} \ln(1 + B_T). \tag{8}$$

In the model suggested by Sazhin et al. (2014), Expressions (6) and (2) replaced the traditional Expressions (1) and (4). The former model was referred to as Model 2 while the latter was referred to as Model 1. One of the attractive features of Model 2 is that it does not use Expression (1) which was derived using a rather stringent assumption that ρ_{total} is constant. Note that B_T in Expression (8) is taken from the previous timestep to avoid the iteration process.

The predictions of Models 1 and 2 were compared by Sazhin et al. (2014) for conditions typical of Diesel engines. It was demonstrated that although both models predict similar trends of time evolution of $\dot{q}_d$, actual predicted values of $\dot{q}_d$ were visibly different. Similar differences were observed for droplet radii, surface temperatures, and evaporation times. These differences were expected due to the different assumptions on which these models were based. Unfortunately, specific recommendations regarding the range of applicability of Models 1 and 2 could not be inferred from the analysis presented by Sazhin et al. (2014).

Recently, a new model of droplet heating and evaporation was suggested which is believed to be more advanced compared with the above-mentioned Models 1 and 2 (Antonov et al., 2023). $\dot{q}_d$ in this model is inferred from Expression (6), as in Model 2. The evaporation rate used in this model is obtained from the numerical solution to equation (Tonini and Cossali, 2012):

$$\hat{m}_e + \left[\tilde{T}_s - 1\right] \left(\frac{\hat{m}_e}{1 - \exp\left(-\frac{\hat{m}_e}{\mathrm{Le}}\right)} - \mathrm{Le} \right) = -\mathcal{P} \hat{p}_{v,\mathrm{cr}}, \tag{9}$$

Table 1
Summary of equations used in Models 1–3 and primary focuses of these models.

Model	Equations used	Primary focus of the model
1	(1), (4)	Evaporation rate (Eq. (1))
2	(6), (2)	Heating rate (Eq. (6))
3	(9), (6)	Evaporation rate (Eq. (9))

where

$$\mathcal{P} = \ln\left[(\hat{p}_{v,\mathrm{cr}} - \hat{p}_{vs}) \times (\hat{p}_{v,\mathrm{cr}} - Y_{v\infty})^{-1}\right],$$

$$\hat{p}_{v,\mathrm{cr}} = 1 + \theta(1 - Y_{v\infty}), \quad \theta_{\mathrm{TC}} = \frac{M_v - M_g}{M_g}, \quad \hat{p}_{vs} = \frac{p_{vs} M_v}{R_u T_{g\infty} \rho_{g\infty}},$$

$$\hat{m}_e = \frac{|\dot{m}_d|}{4\pi R_d D_v \rho_{g\infty}},$$

R_u is the universal gas constant, p_{vs} is the saturation vapour pressure at $T = T_s$, and M_g and M_v are the molar masses of ambient gas (air) and vapour, respectively.

Eq. (9) can be used when:

$$\varepsilon = \frac{M_v D_v^2}{R_u T_{g\infty} R_d^2} \ll 1. \tag{10}$$

Rigorous proof of Eq. (9) when (10) is valid was presented by Tonini et al. (2022). Eq. (9) was derived based on the one-dimensional conservation equations without assuming that the gas mixture has constant density (the derivation of (1) was based on this assumption). Eq. (1) follows from (9) for constant density of the gas mixture. The model using Expression (6) and Eq. (9) is hereafter called Model 3. The equations used in Models 1–3 and primary focuses of the models are summarised in Table 1.

To summarise the main features and limitations of Models 1–3, the primary focus of Model 1 is on Eq. (1) which was derived using a rather restrictive assumption that $\rho_{\mathrm{total}} = \rho_g + \rho_v$ does not depend on the distance from the droplet surface. This assumption is expected to be acceptable for weak evaporation but can be restrictive for strong evaporation when ρ_{total} is controlled mainly by ρ_v near the droplet surfaces and ρ_g in the ambient gas. The heating rate of droplets in this model ($\dot{q}_d$) is inferred from the balance of mass and heat fluxes in the gas phase, and is assumed to be constant at each time step. The physical mechanism of $\dot{q}_d$ is not considered in this model.

The primary focus of Model 2 is on Expression (6), inferred from the analytical solution to the heat transfer equation inside droplets with the Robin boundary condition at their surfaces, which gives the time evolution of droplet heating during each time step. The value of $\dot{q}_d$ at the end of the time step is used as the initial value at the following time step with updated values of the input parameters. The substitution of this value into (2) gives the required droplet evaporation rate. Note that Expression (2) was derived from the balance of the heat fluxes in the gas phase without considering the physical nature of the evaporation process.

The primary focus of Model 3 is on Eq. (9) which gives an implicit expression for the droplet evaporation rate. In contrast to Expression (1), the evaporation rate which is inferred from Eq. (9) does not rely on the assumption that $\rho_{\mathrm{total}} = \rho_g + \rho_v$ is independent of the distance from the droplet surface, and this makes it applicable over a rather wide range of evaporation rates. As in Model 2, $\dot{q}_d$ is calculated directly from the analytical solution to the heat transfer equation inside the droplets with the Robin boundary condition at their surfaces. In contrast to Model 2, in Model 3, the value of $\dot{q}_d$ is not used for the estimation of the droplets' evaporation rate. Thus Model 3 is based on direct analysis of the heat transfer and evaporation processes without using the rather restrictive assumptions upon which Models 1 and 2 are based.

Although Model 3 has clear advantages compared with Models 1 and 2, its practical applicability has been restricted by its complexity. Instead of using a simple explicit expression for $\dot{m}_d$ (Expressions (1) or (2)) it requires numerical solution of a rather complex Eq. (9). Thus, users are likely to be tempted to adopt the relatively simple, although less accurate Models 1 or 2 instead of the more rigorous Model 3. This can be justified provided that the range of applicability of Models 1 and 2 has been identified. We have attempted to do this in the current paper.

In all three models, the temperature dependencies of thermophysical properties were considered in both liquid and gas phases (provided that ρ_{total} does not depend on the distance from the droplet surface in Model 1), and surface temperature distribution was assumed to be homogeneous. If the models are applied to moving droplets and the Effective Thermal Conductivity (ETC) model (Sazhin, 2022) is used then the droplet surface temperature T_s refers to the average droplet surface temperature.

The aim of this paper is to generalise the analysis presented by Sazhin et al. (2014), based upon the comparison between the predictions of Models 1 and 2, to the one based upon the comparison between the predictions of Models 1, 2, and 3.

2. Numerical algorithm

Models 1, 2, and 3, described in Section 1, were implemented in the Matlab R2020a based numerical algorithm. 150 terms were used in the series in Expression (6). A timestep of 0.00001 s was used in the calculations. 100000 concentric layers were used to calculate the integrals in the expression for Expression q_n in (6). Eq. (7) was solved based on the bisection method with absolute errors not exceeding 10^{-12}.

The calculations were performed using the following steps:

1. A distribution of the temperature in the droplet is assumed or the one obtained at the previous timestep is used.
2. The average temperature in the droplet is calculated.
3. The liquid thermophysical properties at this temperature are obtained.
4. The value of the effective thermal conductivity is obtained.
5. The transport and thermodynamic properties of the ambient gas/vapour mixture at the reference temperature (using the '1/3 rule' (Sazhin, 2022)) are calculated.
6. The rate of droplet evaporation is obtained.
7. The Nusselt number (Nu= $2hR_d/k_g$) and the convective heat transfer coefficient (h) are obtained.
8. The temperature distribution in the droplet is inferred from the corresponding analytical solution for the liquid phase if required.
9. Droplet radius at the end of the timestep is re-calculated, considering its swelling and evaporation.
10. The process is repeated by returning to Step 1 if required.

3. Verification of the models

Our first step in the verification of the numerical algorithm presented in Section 2 focuses on a comparison of droplet surface temperatures T_s and heat rates $\dot{q}_d$ predicted by the new algorithm and the one developed by Sazhin et al. (2014). The results are presented in Fig. 1 for the input parameters summarised in Table 2. As can be seen in Fig. 1, the values of T_s and $\dot{q}_d$ predicted by these algorithms coincide within the accuracy of plotting except at the final stage of droplet evaporation when droplet initial volume is reduced by more than 99.9%. The problems with accurately modelling droplet heating and evaporation at this stage of the process are well known (Sazhin, 2022). Apart from this relatively minor issue, we can conclude that this matching for Models 1 and 2 supports the reliability of these models for practical engineering applications.

The verification of the new algorithm with Model 3 is based on the comparison of its predictions, in the limiting case of large liquid thermal conductivity, with the results presented by Tonini and Cossali

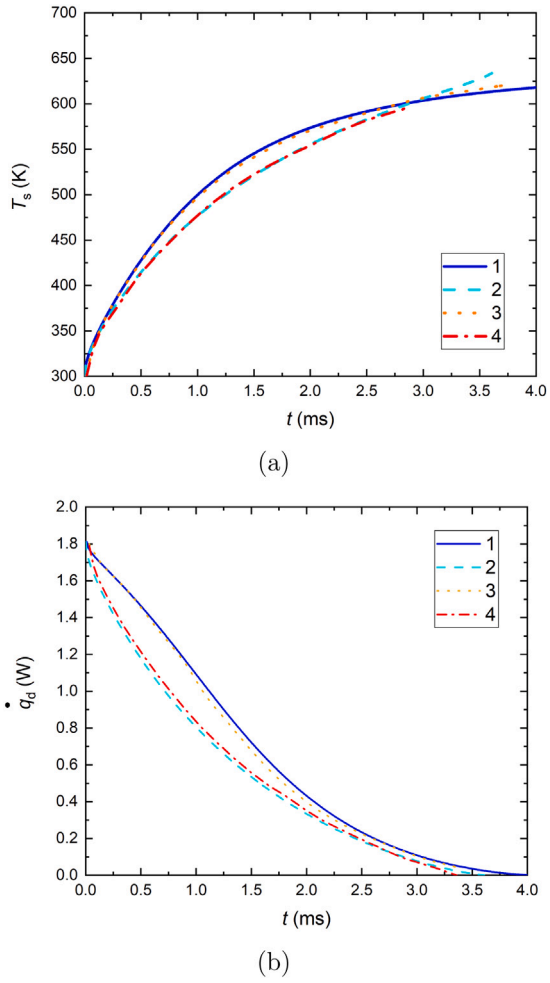

Fig. 1. Plots of droplet surface temperature (a) and heating rate (b) versus time predicted by Model 1 (curves 1 and 3) and Model 2 (curves 2 and 4). Curves 1 and 2 refer to the results obtained by the new MATLAB algorithm; curves 3 and 4 are reproduced from Sazhin et al. (2014). In both cases, input parameters presented in Table 2 were used.

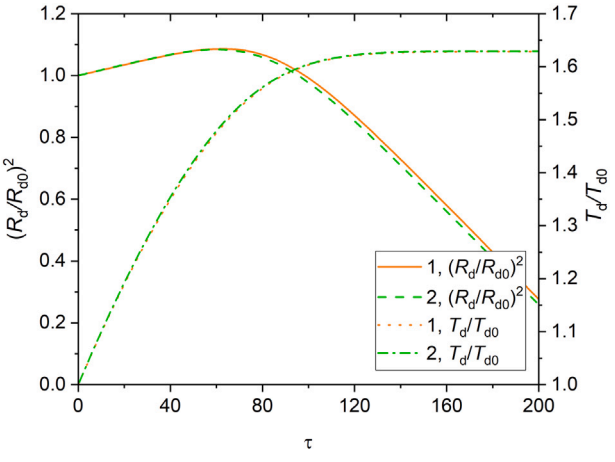

Fig. 2. Plots of non-dimensional droplet radii squared $(R_d/R_{d0})^2$ and volume average temperatures T_d/T_{d0} versus normalised time $\tau = tD_{v0}/R_{d0}^2$, where D_{v0} is the vapour diffusion coefficient at the initial droplet temperature T_{d0}, predicted by the numerical algorithm based upon Model 3, assuming that the thermal conductivity of liquid is equal to 1 kW/(m K) (Curves 1) and the values of $(R_d/R_{d0})^2$ and T_d/T_{d0} reproduced from Tonini and Cossali (2012) (Curves 2). In both cases, input parameters presented in Table 3 were used.

Table 2
Input parameters based upon which the plots shown in Fig. 1 were obtained.

Parameter	Value
R_{d0} (Initial droplet radius)	10^{-5} m
T_0 (Initial droplet temperature)	300 K
T_∞ (Ambient temperature)	700 K
p (Ambient gas pressure)	30 bar
R_u (Universal gas constant)	8.3154 J/(K mol)
M_v (Molar mass of n-dodecane)	0.17033 kg/mol
M_a (Molar mass of air)	0.02897 kg/mol
T_{cr} (Critical n-dodecane temperature)	659 K

Table 3
Input parameters based upon which the plots shown in Fig. 2 were obtained.

Parameter	Value
R_{d0} (Initial droplet radius)	10^{-5} m
T_0 (Initial droplet temperature)	300 K
T_∞ (Ambient temperature)	600 K
p (Ambient gas pressure)	101325 Pa
M_v (Molar mass of n-hexadecane)	$226.446 \cdot 10^{-3}$ kg/mol
T_{cr} (Critical n-hexadecane temperature)	723 K

(2012) in the same limiting case (in both cases, the same gas phase model was used). The results of the comparison for $(R_d/R_{d0})^2$ and T_d/T_{d0} versus non-dimensional time $\tau = tD_{v0}/R_{d0}^2$ are shown in Fig. 2. Parameters summarised in Table 3 were used in the new algorithm and in Tonini and Cossali (2012). As follows from Fig. 2, the values of T_d/T_{d0} and $(R_d/R_{d0})^2$ obtained using both algorithms (the new one, for large liquid thermal conductivity, and the one used in Tonini and Cossali (2012)) are very close. This supports the applicability of both algorithms for practical applications.

Thus, our new algorithm is verified for all three models under consideration.

4. Modelling results versus experimental data

The experiments, the results of which were used for preliminary validation of the algorithms developed using Models 1–3, were performed using the same setup as described by Antonov et al. (2023). In contrast to Antonov et al. (2023), the focus of this section is not on the time evolution of droplet radii and average temperatures but on the rates of change of these quantities. It was observed that these rates are particularly sensitive to the choice of models used in the analysis. The air flow velocity in the experiments did not exceed 0.3 m/s which allowed us to ignore the contribution of this velocity in the modelling of the process.

Plots of rates of change of radii ($\dot{R}_d$) and average temperatures ($\dot{T}_d$) of an n-decane droplet versus time, observed experimentally (exp) and predicted by Models 1, 2 and 3, are presented in Fig. 3. Gas temperature T_g was 760 ± 10 K; initial droplet temperature (T_{d0}) and radius (R_{d0}) were 300 ± 10 K and 0.85 ± 0.05 mm, respectively. It can be seen from this figure that the experimentally observed $\dot{R}_d$ and $\dot{T}_d$ are reasonably close to those predicted by Model 3, except at the very end of droplet evaporation. Minor deviations between experimental results and those predicted by Model 3 are associated with a number of assumptions used in numerical simulations (e.g. the assumptions that the droplets can be approximated by perfect spheres and the contribution of the droplet support can be ignored).

The deviations between the observed values of $\dot{R}_d$ and $\dot{T}_d$ and those predicted by Models 1 and 2 are substantial. These models even predict different trends of change for these quantities, which limits their suitability for studying the time evolution of these quantities during droplet heating/evaporation.

The same plots as shown in Fig. 3, but for ambient gas temperature equal to 500 ± 10 K, are presented in Fig. 4. As follows from Fig. 4, the experimentally observed $\dot{R}_d$ and $\dot{T}_d$ are reasonably close to those predicted by Model 3, except at the very end of droplet evaporation, as in the case shown in Fig. 3 for higher ambient gas temperatures.

Table 4
Approximations of thermophysical properties of n-dodecane (p is in Pa; T is in K) (Yaws, 2015).

Property	Approximation
Density (kg/m^3)	$235.1055 \cdot 0.2551^{-(1-T/658.2)^{0.2889}}$
Specific liquid heat capacity (J/(kg K))	$1161.216 + 3.5067 \cdot T$
Thermal liquid conductivity (W/(m K))	$10^{-1.7565+1.0556\cdot(1-T/658.2)^{2/7}}$
Liquid dynamic viscosity (Pa s)	$10^{-10.0687+1253/T+0.0137\cdot T-0.000012215\cdot T^2}$
Latent heat of evaporation (J/kg)	$691.9237 \cdot (658.2 - T)^{0.407}$
Saturation vapour pressure (Pa)	$10^5 \cdot \exp\left(8.1948 - 2342.97/T - 810882.0/T^2\right)$
Binary vapour diffusion coefficient (m^2/s)	$5.27 \cdot 10^{-6} \cdot (T/300)^{1.583} \cdot (p/10^5)^{-1}$
Specific vapour heat capacity (J/(kg K))	$297.9 + 1439.4 \cdot (T/300) - 135.1 \cdot (T/300)^2$
Thermal vapour conductivity (W/(m K))	$0.02667 \cdot (T/300) - 0.02087$
Liquid dynamic viscosity (Pa s)	$\left[0.5651 + 1.041 \cdot 10^{-3} \cdot (T - 300)\right] \cdot 10^{-5}$

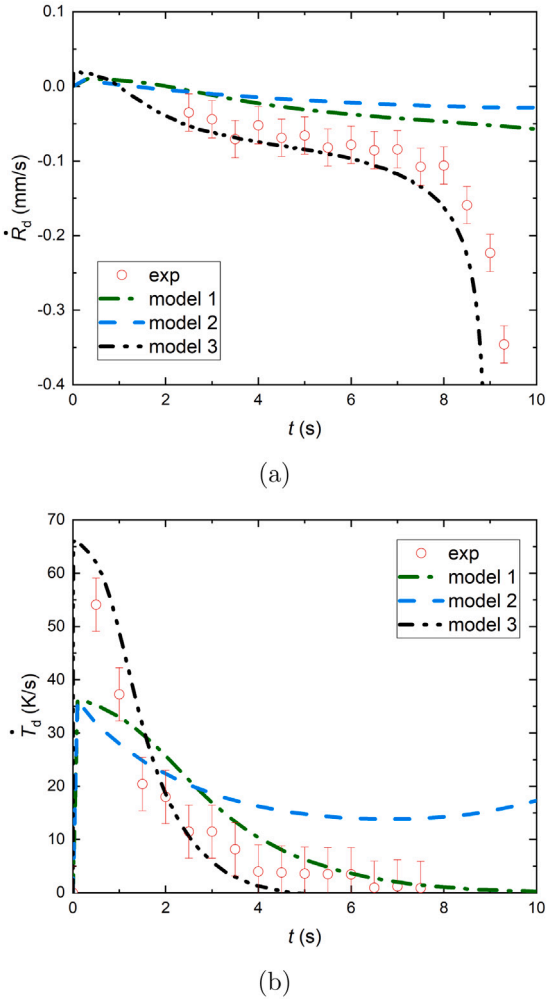

Fig. 3. Plots of rate of change of radius ($\dot{R}_d$) and average temperature ($\dot{T}_d$) of an n-decane droplet versus time observed experimentally (exp) and predicted by Models 1, 2 and 3. Gas temperature T_g was 760 ± 10 K; initial droplet temperature (T_{d0}) and radius (R_{d0}) were 300 ± 10 K and 0.85 ± 0.05 mm, respectively.

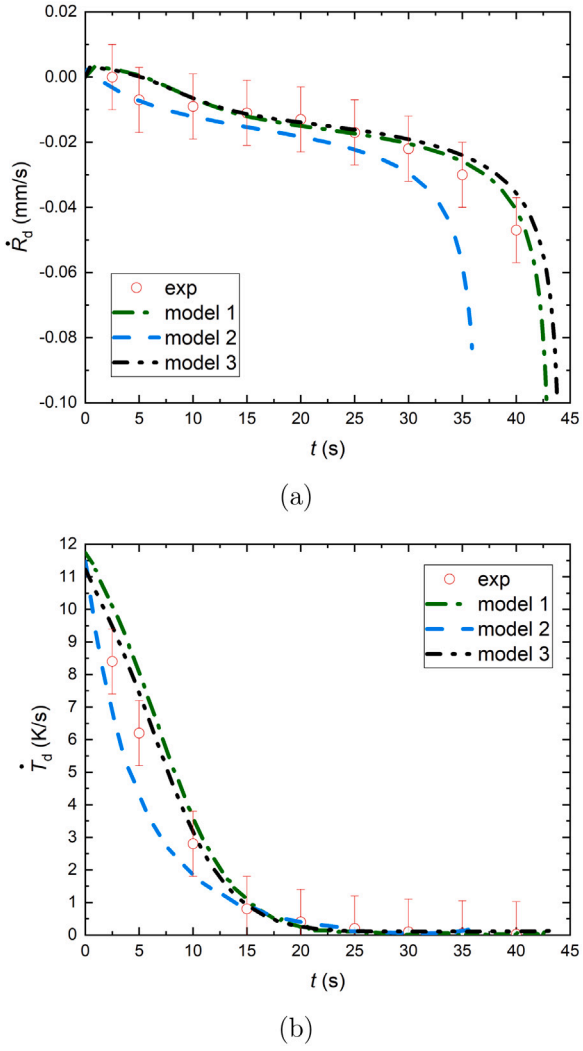

Fig. 4. The same as Fig. 3, but for $T_g = 500 \pm 10$ K.

5. Parametric study

In what follows, the predictions of Models 1, 2 and 3 for a wide range of input parameters, typical for engineering applications, will be compared. The focus will be on n-dodecane droplets. n-dodecane is commonly believed to be a reasonable approximation of Diesel fuel (Sazhin, 2022). Its thermophysical properties, summarised in Table 4, are close to those of some other fuels of engineering importance (e.g. kerosene, petrol) (Sazhin, 2022).

Firstly, we compare the predictions by Models 1 and 2 of the heating rates of droplets with various initial surface and gas temperatures and radii. The plots of normalised heating rates $\dot{q}_d/\dot{q}_{d0}$ versus normalised droplet surface temperatures T_s/T_g, predicted by Models 1 and 2, for $R_{d0} = 10$ μm and several gas temperatures T_g are shown in Fig. 5a. As can be seen in this figure, at gas temperatures greater than 400 K, $\dot{q}_d/\dot{q}_{d0}$ obtained using Models 1 and 2 are rather different, although they show similar trends. This agrees with the results given by Sazhin et al. (2014). At the same time, at gas temperatures less than about 350 K, $\dot{q}_d/\dot{q}_{d0}$ obtained using both models become very close.

Plots of non-dimensional heat rates $\dot{q}_d/\dot{q}_{d0}$ versus normalised droplet surface temperatures T_s/T_g, predicted by Models 1 and 2, for $T_g = 700$ and R_{d0} in the range 1 to 10 μm are presented in Fig. 5b. This figure

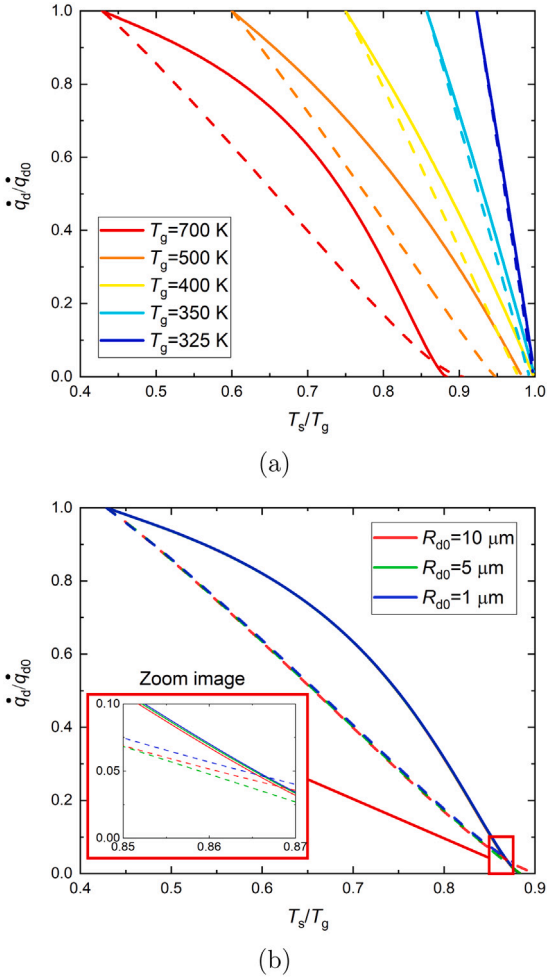

Fig. 5. Plots of normalised heat rate $\dot{q}_d/\dot{q}_{d0}$, predicted by Models 1 (solid) and 2 (dashed), versus normalised droplet surface temperature T_s/T_g for R_{d0} = 10 μm at various gas temperatures T_g (a), and T_g = 700 K with various droplet initial radii R_{d0} (b).

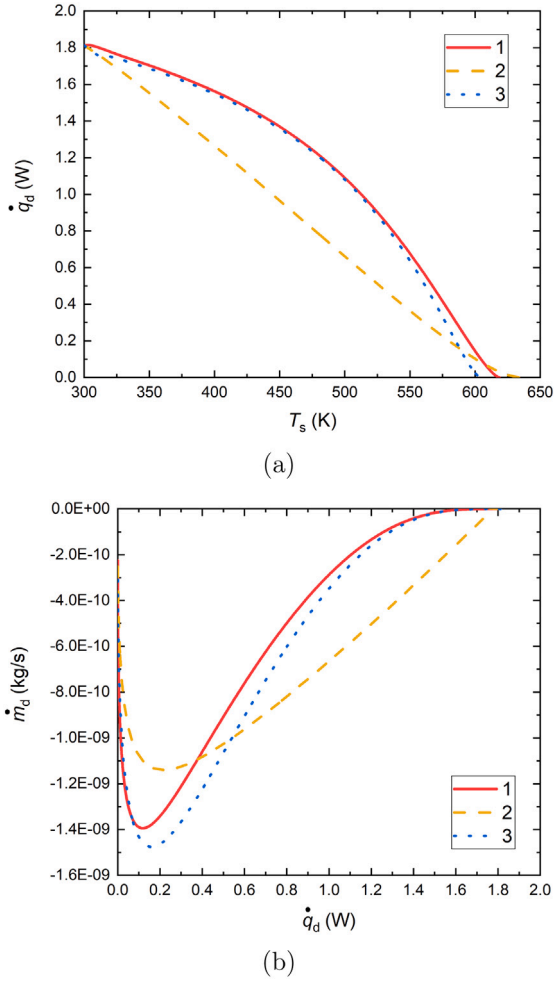

Fig. 6. Plots of $\dot{q}_d$ versus T_s (a), and $\dot{m}_d$ versus $\dot{q}_d$ (b) predicted by Models 1, 2, and 3 (numbers in the insert); parameters given in Table 2 were used.

shows that, for both models, the predicted $\dot{q}_d/\dot{q}_{d0}$ do not depend on R_{d0}.

Plots of $\dot{q}_d$ versus T_s obtained using all three models are presented in Fig. 6a. As one can clearly see from this figure, $\dot{q}_d$ calculated using Model 3 are very close to those obtained using Model 1 for the selected values of parameters. This result is consistent with those described by Tonini and Cossali (2012) where it was shown that droplet lifetimes, calculated using the same gas phase model as in Model 3, are close to those calculated using the same gas phase model as in Model 1 (called the Stefan-Fuchs model by Tonini and Cossali (2012)). The difference between the liquid phase models used in Models 1 and 3 does not have a significant effect on the calculated values of $\dot{q}_d$.

Plots of $\dot{m}_d$ versus $\dot{q}_d$ predicted by all three models are shown in Fig. 6b. As follows from this figure, $\dot{m}_d$ predicted by Model 3 are very close to those predicted by Model 1 for small and large $\dot{q}_d$. There is a relatively small difference between $\dot{m}_d$ predicted by these models for intermediate values of $\dot{q}_d$ which may be acceptable in many engineering applications. Note that large $\dot{q}_d$ are typical for the start of the heating/evaporation process when droplet surface temperatures are low, while small values of $\dot{q}_d$ are typical for the final stage of this process.

Plots of T_s versus time calculated using Models 1, 2, and 3 are presented in Fig. 7a. As can be seen in this figure, T_s calculated using Model 3 are close to those calculated using Model 1, especially at the beginning of the heating/evaporation process. The trends in the time evolution of T_s predicted by Model 2 are similar to those predicted by Models 1 and 3, although the predicted values of T_s are visibly different except at the very beginning of the evaporation process (the first 0.5 ms).

Plots of $\dot{q}_d(t)$ predicted by Models 1, 2, and 3 are presented in Fig. 7b. As can be seen in this figure, $\dot{q}_d$ calculated using Model 3 are very close to those calculated using Model 1 throughout the whole process. However, the values of this quantity predicted by Model 2 are visibly different from the ones predicted by Models 1 and 3.

Plots of $\dot{m}_d$ versus time calculated using Models 1, 2, and 3 are presented in Fig. 7c. As can be seen in this figure, $\dot{m}_d$ predicted by Model 3 are rather close to those calculated using Model 1 but clearly different from those calculated using Model 2.

Fig. 7 demonstrates that a relatively simple Model 1 can replace a more complex Model 3 for the selected values of parameters. The predictions of Model 2 for these parameters are expected to introduce large errors in predicted characteristics of the process. The practical applicability of this model for these values of input parameters is therefore questionable.

The same plots as in Fig. 7 but for T_g = 325 K are presented in Fig. 8. As follows from Figs. 8a and 8b, T_s and $\dot{q}_d$ calculated using Models 1 and 2 almost coincide, in agreement with the results presented in Fig. 5. The values of T_s and $\dot{q}_d$ calculated using Model 3 almost coincide with those predicted by Models 1 and 2 at the beginning of the process (t less than about 3 ms). At the final stage of the process, however, T_s

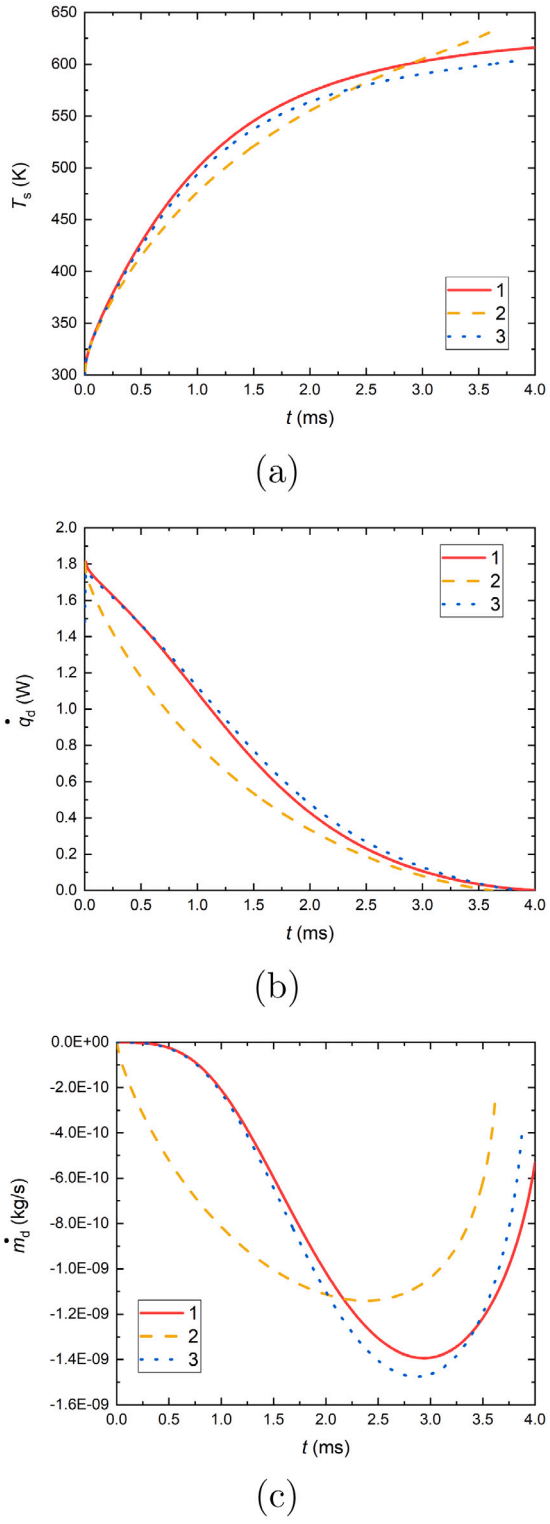

Fig. 7. Plots of T_s (a), $\dot{q}_d$ (b), and $\dot{m}_d$ (c) versus time predicted by Models 1, 2, and 3 (numbers in the inserts) for T_g = 700 K and the remaining input parameters as presented in Table 2.

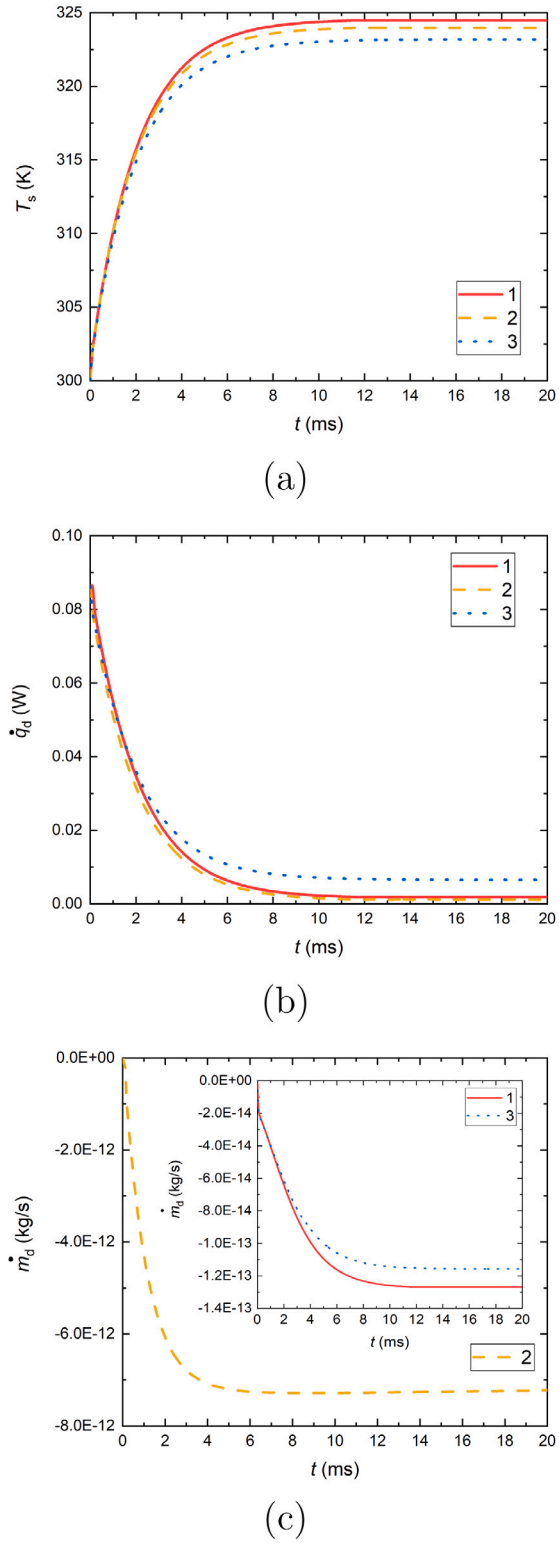

Fig. 8. The same as Fig. 7 but for T_g = 325 K.

calculated using Model 3 is slightly lower than that calculated using Models 1 and 2, and $\dot{q}_d$ calculated using Model 3 is slightly higher than that calculated using Models 1 and 2.

It can be seen from Fig. 8c that $\dot{m}_d$ calculated using Models 1 and 3 are reasonably close, but both are more than an order of magnitude higher than those predicted by Model 2. In all cases, however, the predicted values of $\dot{m}_d$ are more than about two orders of magnitude lower than those shown in Fig. 7c. Thus, we can safely ignore the contribution of the evaporation process in this case in most applications.

As can be seen in Figs. 7 and 8, a relatively simple Model 1 can replace a more complex Model 3 for gas temperatures up to about 700 K, unless very accurate calculations are required.

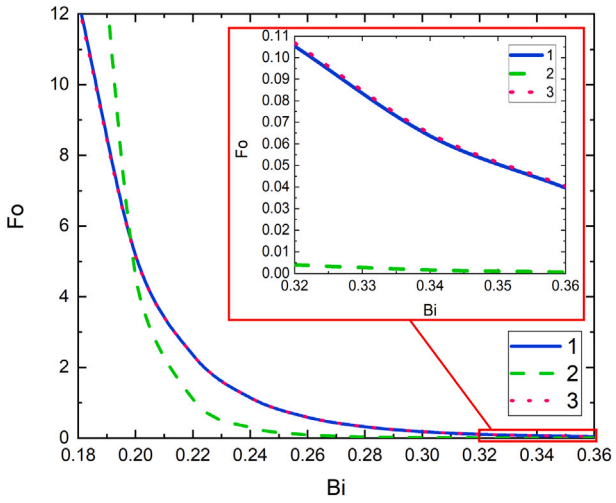

Fig. 9. Plots of Fourier number Fo= $t_e\kappa_l/R_{d0}^2$ versus Biot number Bi= hR_{d0}/k_{l0} predicted by Models 1, 2 and 3 (the keys show the model numbers).

Plots of normalised evaporation time (Fourier number) versus normalised convective heat transfer coefficient (Biot number), inferred from parametric study of n-dodecane droplet heating/evaporation in a wide range of droplet radii 10 μm to 1 mm and gas temperatures 400 K to 1000 K, are presented in Fig. 9. As Fig. 9 shows, all three models predict decreasing Fo with increasing Bi. The results predicted by Models 1 and 3 are practically indistinguishable.

6. Conclusions

Three approaches to modelling the heating and evaporation of monocomponent droplets are compared. Firstly, the heat rate supplied to the droplets to heat them up, $\dot{q}_d$, is inferred from the requirement that the droplet evaporation rates $\dot{m}_d$, obtained from the heat and mass balance equations in the gas phase, should be equal. In the second approach, $\dot{q}_d$ is calculated directly using the analytical solution to the heat transfer equation in a spherical droplet. This value of $\dot{q}_d$ is then used for the estimation of the Spalding heat transfer number and $\dot{m}_d$. The third approach uses the same algorithm for the calculation of $\dot{q}_d$ as the second approach, but the mass evaporation rate is inferred from the coupled solution to the conservation equations in the gas phase.

Numerical algorithms using these three approaches are developed. The predictions of the algorithms based on the first two approaches are verified using the previously developed algorithms. The predictions of the algorithm using the third approach are verified based on the comparison of its predictions with those of the previously developed algorithm for the case of infinitely high liquid thermal conductivity.

The predictions of all three algorithms are compared with experimentally observed time dependencies of the rates of change of average temperatures and radii of n-decane droplets at initial temperatures and radii equal to 300 K and 0.85 mm, respectively, introduced in air at temperatures 500 K and 760 K. It is shown that the predictions of these quantities using the algorithm based on the third approach are close to the experimental data. Noticeable deviations were observed between experimental data and predictions of these rates by the other two algorithms.

The predictions of the algorithms using these three approaches are compared for parameters that are typical for engineering applications. The focus is on n-dodecane droplets. It is shown that the predictions of the algorithms using the first two approaches are close for low gas temperatures (close to room temperatures). In the general case, the predictions of the algorithm for the third approach are closer to those for the first approach than to those for the second. Thus, the present study shows that Model 1 is generally sufficient for an adequate prediction of the evaporation and heating rates under the conditions prevalent in most engineering application.

CRediT authorship contribution statement

Dmitrii V. Antonov: Writing – review & editing, Visualization, Validation, Software, Resources, Methodology, Investigation, Formal analysis, Data curation. **Simona Tonini:** Writing – review & editing, Software, Resources, Methodology, Investigation, Formal analysis. **Gianpietro Elvio Cossali:** Writing – review & editing, Software, Resources, Methodology, Investigation, Formal analysis. **Mansour Al Qubeissi:** Writing – review & editing, Software, Methodology, Investigation. **Pavel A. Strizhak:** Writing – review & editing, Validation, Supervision, Methodology. **Sergei S. Sazhin:** Writing – review & editing, Writing – original draft, Supervision, Investigation, Formal analysis, Conceptualization.

Declaration of competing interest

The work described has not been published previously and it is not under consideration for publication elsewhere. Its publication is approved by all authors and tacitly or explicitly by the responsible authorities where the work was carried out. If accepted, it will not be published elsewhere in the same form, in English or in any other language, including electronically without the written consent of the copyright-holder.

Data availability

Data will be made available on request.

Acknowledgements

Research was supported by the Russian Science Foundation (Grant 24-45-00012, https://rscf.ru/project/24-45-00012/), the University of Bergamo (SS's visiting professorship) and the Royal Society (UK) (Grant IEC 192007).

References

Abramzon, B., Sirignano, W.A., 1989. Droplet vaporization model for spray combustion calculations. Int. Commun. Heat Mass Transfer 32, 1605–1618. http://dx.doi.org/10.1016/0017-9310(89)90043-4.

Aliseda, A., Hopfinger, E.J., Lasheras, J.C., Kremer, D.M., Berchielli, A., Connolly, E.K., 2008. Atomization of viscous and non-Newtonian liquids by a coaxial, high-speed gas jet. Experiments and droplet size modeling. Int. J. Multiph. Flow 34 (2), 161–175. http://dx.doi.org/10.1016/j.ijmultiphaseflow.2007.09.003.

Antonov, D.V., Tonini, S., Cossali, G.E., Dolgikh, V.V., Strizhak, P.A., Sazhin, S.S., 2023. Droplet heating and evaporation: a new approach to the modelling of the processes. Phys. Fluids 35, 073311. http://dx.doi.org/10.1063/5.0158661.

Barrow, H., Pope, C.W., 2007. Droplet evaporation with reference to the effectiveness of water-mist cooling. Appl. Energy 84, 404–412. http://dx.doi.org/10.1016/j.apenergy.2006.09.007.

Fan, J.-N., Qiao, M., Yang, Y., Wang, Y., et al., 2024. Mathematical modeling of multicomponent aerosol droplet evaporation and growth in indoor environments. J. Hazard. Mater. 474, 134837. http://dx.doi.org/10.1016/j.jhazmat.2024.134837.

Fuchs, N.A., 1959. Evaporation and Droplet Growth in Gaseous Media. Pergamon Press.

Kitano, T., Nishio, J., Kurose, R., Komori, S., 2014. Effects of ambient pressure, gas temperature and combustion reaction on droplet evaporation. Combust. Flame 161, 551–564. http://dx.doi.org/10.1016/j.combustflame.2013.09.009.

Kumar, R., Tijerino, E., Saha, A., Basu, S., 2010. Structural morphology of acoustically levitated and heated nanosilica droplet. Appl. Phys. Lett. 97 (12), 123106. http://dx.doi.org/10.1063/1.3493178.

Saha, K., Abu-Ramadan, E., Li, X., 2012. Multicomponent evaporation model for pure and blended biodiesel droplets in high temperature convective environment. Appl. Energy 93, 71–79. http://dx.doi.org/10.1016/j.apenergy.2011.05.034.

Sazhin, S.S., 2022. Droplets and Sprays: Simple Models of Complex Processes. Springer, http://dx.doi.org/10.1007/978-3-030-99746-5.

Sazhin, S.S., Al Qubeissi, M., Xie, J.-F., 2014. Two approaches to modelling the heating of evaporating droplets. Int. Commun. Heat Mass Transfer 57, 353–356. http://dx.doi.org/10.1016/j.icheatmasstransfer.2014.08.004.

Spalding, D.B., 1963. Convective Mass Transfer; An Introduction. Edward Arnold Ltd, London.

Tonini, S., Cossali, G.E., 2012. An analytical model of liquid drop evaporation in gaseous environment. Int. J. Therm. Sci. 57, 45–53. http://dx.doi.org/10.1016/j.ijthermalsci.2012.01.017.

Tonini, S., Cossali, G.E., Shchepakina, E.A., Sobolev, V.A., Sazhin, S.S., 2022. A model of droplet evaporation: new mathematical developments. Phys. Fluids 34, 073312. http://dx.doi.org/10.1063/5.0098331.

Vehring, R., Foss, W.R., Lechuga-Ballesteros, D., 2007. Particle formation in spray drying. J. Aerosol Sci. 38 (7), 728–746. http://dx.doi.org/10.1016/j.jaerosci.2007.04.005.

Wolf, S.E., Leiterer, J., Kappl, M., Emmerling, F., Tremel, W., 2008. Early homogeneous amorphous precursor stages of calcium carbonate and subsequent crystal growth in levitated droplets. J. Am. Chem. Soc. 130 (37), 12342–12347. http://dx.doi.org/10.1021/ja800984y.

Xi, X., Cai, C., Liu, H., Wen, R., Ma, X., Song, X., 2023. Analytical and experimental study on binary droplet evaporation: Inhibitory effect of adding mineral oil adjuvant to water. Int. Commun. Heat Mass Transfer 142, 106630. http://dx.doi.org/10.1016/j.icheatmasstransfer.2023.106630.

Yaws, C., 2015. Transport Properties of Chemicals and Hydrocarbons. Gulf Professional Publishing.

Zhang, Z., Zhao, H., Vanapalli, S., 2024. Modeling of a liquid nitrogen droplet evaporating inside an immiscible liquid pool. Int. Commun. Heat Mass Transfer 226, 125444. http://dx.doi.org/10.1016/j.ijheatmasstransfer.2024.125444.